Int. J. Heat Mass Transfer. Vol. 34, No. 6, pp. 1503–1513, 1991
Printed in Great Britain

0017–9310/91 $3.00 + 0.00

Application of weighting function scheme on convection–conduction phase change problems

W. Y. RAW and S. L. LEE

Department of Power Mechanical Engineering, National Tsing-Hua University, Hsinchu, Taiwan 30043, Republic of China

(*Received* 3 *October* 1989 *and in final form* 12 *July* 1990)

Abstract—A numerical formulation based on the weighting function scheme is developed in the present investigation for convection–conduction phase change problems. The solid phase is regarded as a liquid having an infinite viscosity. Such a treatment allows the stream–vorticity formulation to apply over the entire physical domain including the liquid–solid interface. The weighting function scheme then is used to handle the sharp viscosity jump at the liquid–solid interface. A problem dealing with pure tin is employed to test the performance of the present method. The predicted interface profiles are found to agree with available experimental data qualitatively. The computation effort required by the present numerical technique, however, is less than 2% of that needed by a two-region method for this same problem. Unlike the existing single-region methods, the present numerical technique produces smooth streamlines and isotherms even in the vicinity of the solidification front.

INTRODUCTION

IT HAS been well recognized that natural convection in the liquid phase of a phase change material (PCM) could have a significant effect on the moving speed and the shape of the liquid–solid interface [1–3]. This is true even for liquid metals that possess small Prandtl numbers. To study the effect of natural convection on phase change processes, many numerical investigations [4–15] have been performed. The numerical techniques employed in these studies can be classified into two-region [4–8] and single-region [9–15] methods.

In two-region methods, two independent sets of conservation equations are derived for each of the liquid and solid phases. An appropriate energy balance at the liquid–solid interface then is employed to couple the two sets of governing equations. Such a numerical formulation produces smooth isotherms and streamlines in the vicinity of the liquid–solid interface. However, the liquid–solid interface has an irregular shape varying from time to time in most practical phase change problems. Under this situation, both liquid and solid phases might have irregular domains with a Dirichlet boundary condition at the liquid–solid interface. Hence, an algebraic coordinates transformation [4–7] or boundary-fitted curvilinear coordinates [8] is needed for each of the liquid and solid regions. This renders the use of the two-region methods very complicated. Therefore, some simplification dealing with the geometric regularity of the interface is generally needed as demonstrated by Sparrow *et al.* [4]. In addition, the governing equations based on a two-region method will become singular when either the liquid or solid phase does not exist. Thus, additional assumptions such as used in refs. [5, 16] are needed at the very beginning and the final step of the solidification process.

To circumvent the numerical difficulties encountered in the use of the two-region formulations, a few single-region methods such as refs. [9–15] have been developed. In these single-region methods, the evolution of the latent heat during the solidification process is embedded in the local enthalpy change rate $\partial H/\partial t$. Such a treatment has been proven to automatically satisfy the conventional energy balance condition at the liquid–solid interface [17]. Therefore, a single set of governing equations can be applied on the entire physical domain including the liquid–solid interface. The method proposed by Schneider [9] was derived by introducing a method for fluid flow [18] into the enthalpy-like model [19]. Voller and co-workers [10, 11] separated the latent heat from the sensible heat such that the sensible heat became a continuous function across the liquid–solid interface. This treatment allowed the well-known SIMPLE algorithm [20] to be implemented in their enthalpy formulation. Bennon and Incropera [12, 13] developed a continuum model by integrating semi-empirical laws with classical mixture theory. The mushy zone was formulated as a porous medium. Depending on the value of the liquid fraction, the permeability has a positive finite value in the mushy zone. The value of permeability is zero in the solid phase and becomes infinite in the liquid. A similar volume-averaged formulation was proposed by Beckermann and Viskanta [14] for phase change in porous media. This model is able to handle phase change in a PCM without a porous matrix, if the porosity is assigned unity. Based on the enthalpy method developed in refs. [10, 11], Brent *et al.* [15] proposed the enthalpy–porosity technique by treating

NOMENCLATURE

a	weighting factor defined in equation (12)
a_R	right-hand side of equation (12)
C_P	specific heat at constant pressure [J kg^{-1} K^{-1}]
c_p	dimensionless specific heat, $C_P/(C_P)_l$
f	dimensionless latent heat or fraction of liquid phase, $(H-\Lambda)/\Delta H$
g	gravitational acceleration, 9.81 m s^{-2}
Gr	Grashof number, $\beta g(T_0-T_f)L^3(\rho/\mu_l^*)^2$
Gr^*	modified Grashof number, $(\Lambda_0-\Lambda_z)(T_0-T_f)^{-1}(C_p)_l^{-1}\,Gr$
H	total enthalpy [J kg^{-1}]
ΔH	latent heat [J kg^{-1}]
k	thermal conductivity [W m^{-1} K^{-1}]
L	width of the enclosure
P	static pressure [N m^{-2}]
p	dimensionless pressure, $P\rho(L/\mu_l^*)^2$
Pr	Prandtl number, μ^*/κ
S	height of the enclosure
s	aspect ratio of the enclosure, S/L
Ste	Stefan number, $(\Lambda_0-\Lambda_z)/\Delta H$
T	temperature [°C]
T_0, T_z	reference temperatures [°C]
t	time
t_c	characteristic time, $\rho L^2/(\sigma\kappa_l)$
U, V	velocities in the x- and y-directions, respectively [m s^{-1}]
u, v	dimensionless velocities, U/V_c and V/V_c, respectively
V_c	characteristic velocity, $\mu_l^*/(\rho L)$
X, Y	horizontal and vertical coordinates [m]
x, y	dimensionless coordinates, X/L and Y/L, respectively
Δx, Δy	step sizes in x- and y-coordinates, respectively.

Greek symbols

α	dimensionless dynamic thermal diffusivity, κ/κ_l
β	volumetric coefficient of thermal expansion [K^{-1}]
γ	artificial viscosity for the stream function
ε	tolerance in convergence criterion
η	dimensionless local orthogonal coordinate normal to the liquid–solid interface, see Fig. 3
θ	dimensionless temperature in the liquid, $(T-T_f)/(T_0-T_f)$
κ	dynamic thermal diffusivity, k/C_P
Λ	sensible heat, $\int_{T_z}^{T} C_P\,dT$ [J kg^{-1}]
Λ_z	sensible heat at T_z [J kg^{-1}]
λ	dimensionless sensible heat, $(\Lambda-\Lambda_z)/(\Lambda_0-\Lambda_z)$
μ	dimensionless dynamic viscosity, μ^*/μ_l^*
μ^*	dynamic viscosity [kg m^{-1} s^{-1}]
ξ	dimensionless local orthogonal coordinate tangent to the liquid–solid interface, see Fig. 3 [m]
ρ	density [kg m^{-3}]
σ	$Ste/(1+Ste)$
τ	dimensionless time, t/t_c
ϕ	local inclination angle of the interface
ψ	dimensionless stream function, $u=\partial\psi/\partial y$ and $v=-\partial\psi/\partial x$
ω	dimensionless vorticity, $\partial u/\partial y-\partial v/\partial x$.

Superscript

0	solution at the previous iteration.

Subscripts

E	east
f	quantity based on the freezing point T_f
l	property of the liquid phase at the freezing point T_f
N	north
P	point P
S	south
W	west
x, y	partial derivatives with respect to x and y
0	quantity based on T_0 or solution at previous time step τ_0.

the mushy zone as a porous medium. Such an idea is essentially the same as that used in refs. [12, 13]. A survey on recent developments on phase change problems can be found in the review paper by Viskanta [21].

Although the literature on the methodology for single-region formulation is continuously growing, most of them pose serious numerical difficulties. As can be clearly observed from the results presented in the literature, all of the existing single-region methods [9–15] produce zigzag isotherms and streamlines in the vicinity of a liquid–solid interface. This numerical error has been proven to arise from improper handling of the evolution (or absorption) of the latent heat [22]. The poor solution convergence rate encountered in the use of the existing single-region methods might be also attributed to this same reasoning. In the present investigation, the enthalpy method proposed in ref. [22] will be extended such that the effect of natural convection can be taken into account in a PCM having a distinct freezing point. The solid phase is regarded as a liquid that has an infinite viscosity. The weighting function scheme [22] then is used to handle the sharp discontinuity in the viscosity. Physically speaking, in a plane front solidification (or melting) the velocity has a discontinuous gradient at the liquid–solid inter-

face. A velocity gradient exists on the liquid side due to the no-slip condition, whereas the velocity field is identically zero on the solid side. Such a physical phenomenon can be easily implemented through the use of the weighting function scheme [22]. The performance of the present method will be examined by comparing the present prediction with the experimental data of Wolff and Viskanta [7].

THEORETICAL ANALYSIS

In their investigation, Wolff and Viskanta [7] performed an experiment to study a two-dimensional solidification of pure tin (99.99% pure) in a rectangular enclosure. Measurements including the shape of the liquid–solid interface and the temperature distribution in the liquid phase were undertaken for a series of time instants. A numerical solution based on the two-region method of Ramachandran *et al.* [5] was also obtained for the same physical configuration. The results presented in ref. [7] are quite complete indeed as compared to previous works on phase change problems. Thus, it is convenient to employ the problem studied by Wolff and Viskanta [7] to examine the performance of the present method.

Consider a pure liquid tin of uniform temperature T_0 inside a two-dimensional rectangular enclosure ($0 \leqslant X \leqslant L$ and $0 \leqslant Y \leqslant S$) with perfect insulation at both horizontal walls ($Y = 0$ and S). At time $t \geqslant 0$, the temperature of the vertical wall at $X = L$ is cooled to a uniform temperature T_∞ that is below the freezing point T_f of the pure tin, while the other vertical wall ($X = 0$) is maintained at T_0. Solidification thus starts from the cold wall. In the present physical problem, these would be free of thermal and alloy dendrites [23] because the working medium in the liquid phase is a superheated pure substance. Hence, it is reasonable to assume a plane front solidification. This and other assumptions needed in the analysis are listed as follows:

(1) the liquid tin is a Newtonian fluid;

(2) the density of the pure tin is constant in the entire physical domain ($\rho = \rho_l$ = constant) except for the buoyancy term in the momentum equation;

(3) the shrinkage-caused flow is negligibly small as compared to the buoyancy-driven flow;

(4) the Boussinesq approximation is valid;

(5) the flow in the melt is laminar and two-dimensional;

(6) the liquid–solid interface has a smooth profile.

Based on these assumptions and the dimensionless transformation

$$x = X/L, \quad y = Y/L, \quad u = U/V_c, \quad v = V/V_c$$
$$V_c = \mu_l^*/(\rho L), \quad p = P\rho(L/\mu_l^*)^2, \quad \mu = \mu^*/\mu_l^*$$
$$\lambda = (\Lambda - \Lambda_\infty)/(\Lambda_0 - \Lambda_\infty), \quad \alpha = \kappa/\kappa_l$$
$$f = (H - \Lambda)/\Delta H, \quad \tau = t/t_c, \quad t_c = \rho L^2/(\sigma\kappa_l)$$
$$\theta = (T - T_f)/(T_0 - T_f), \quad s = S/L \tag{1}$$

the governing equations can be expressed as [10, 24]

$$\frac{\partial u}{\partial x} + \frac{\partial v}{\partial y} = 0 \tag{2}$$

$$\frac{\sigma}{Pr_l}\frac{\partial u}{\partial \tau} + u\frac{\partial u}{\partial x} + v\frac{\partial u}{\partial y} = -\frac{\partial p}{\partial x} + 2\frac{\partial}{\partial x}\left(\mu\frac{\partial u}{\partial x}\right) + \frac{\partial}{\partial y}\left(\mu\frac{\partial u}{\partial y}\right) + \frac{\partial}{\partial y}\left(\mu\frac{\partial v}{\partial x}\right) \tag{3}$$

$$\frac{\sigma}{Pr_l}\frac{\partial v}{\partial \tau} + u\frac{\partial v}{\partial x} + v\frac{\partial v}{\partial y} = Gr\,\theta - \frac{\partial p}{\partial y} + \frac{\partial}{\partial x}\left(\mu\frac{\partial v}{\partial x}\right) + 2\frac{\partial}{\partial y}\left(\mu\frac{\partial v}{\partial y}\right) + \frac{\partial}{\partial x}\left(\mu\frac{\partial u}{\partial y}\right) \tag{4}$$

$$(1-\sigma)\frac{\partial f}{\partial \tau} + \sigma\frac{\partial \lambda}{\partial \tau} + Pr_l\, u\frac{\partial \lambda}{\partial x} + Pr_l\, v\frac{\partial \lambda}{\partial y} = \frac{\partial}{\partial x}\left(\alpha\frac{\partial \lambda}{\partial x}\right) + \frac{\partial}{\partial y}\left(\alpha\frac{\partial \lambda}{\partial y}\right). \tag{5}$$

The associated boundary conditions are

$$u = 0, \quad v = 0, \quad \lambda = 1 \qquad \text{at } \tau = 0$$
$$u = 0, \quad v = 0, \quad \lambda = 1 \qquad \text{at } x = 0 \text{ and } \tau > 0$$
$$u = 0, \quad v = 0, \quad \lambda = 0 \qquad \text{at } x = 1 \text{ and } \tau > 0$$
$$u = 0, \quad v = 0, \quad \partial\lambda/\partial y = 0 \qquad \text{at } y = 0 \text{ and } \tau > 0$$
$$\partial u/\partial y = 0, \quad v = 0, \quad \partial\lambda/\partial y = 0 \qquad \text{at } y = s \text{ and } \tau > 0. \tag{6}$$

In equations (3)–(5), the parameters Pr_l, Gr and σ are defined by

$$Pr_l = \mu_l^*/\kappa_l = Pr(T_f^+)$$
$$Gr = \rho^2 g\beta(T_0 - T_f)L^3/(\mu_l^*)^2$$
$$\sigma = Ste/(1 + Ste), \quad Ste = (\Lambda_0 - \Lambda_\infty)/\Delta H. \tag{7}$$

As remarked by Wolff and Viskanta [7], a free surface forms on the top of the melt region at $\tau > 0$ due to the shrinkage of the pure tin (about 4.2%) when solidified. Hence, in equations (6) a no-shear boundary condition is assumed at $y = s$. It is noted that equations (3), (4) and the velocity boundary conditions specified in equations (6) will reduce to $u = v = 0$ if an infinite value is assigned to the viscosity. Thus, the system of governing equations (2)–(6) is valid also in the solid phase as long as the solid is regarded as a liquid of infinite viscosity.

To simplify the problem, the pressure is eliminated from equations (3) and (4) to yield

$$\frac{\sigma}{Pr_l}\frac{\partial\omega}{\partial\tau}+(u-\mu_x)\frac{\partial\omega}{\partial x}+(v-\mu_y)\frac{\partial\omega}{\partial y}$$
$$=\frac{\partial}{\partial x}\left(\mu\frac{\partial\omega}{\partial x}\right)+\frac{\partial}{\partial y}\left(\mu\frac{\partial\omega}{\partial y}\right)-\left[Gr^*(c_p)^{-1}\frac{\partial\lambda}{\partial x}\right.$$
$$\left.+(\mu_{xx}-\mu_{yy})\left(\frac{\partial u}{\partial y}+\frac{\partial v}{\partial x}\right)-2\mu_{xy}\left(\frac{\partial u}{\partial x}-\frac{\partial v}{\partial y}\right)\right] \quad (8)$$

$$\frac{\partial}{\partial x}\left(\gamma\frac{\partial\psi}{\partial x}\right)+\frac{\partial}{\partial y}\left(\gamma\frac{\partial\psi}{\partial y}\right)=f\omega \quad (9)$$

where the stream function ψ is defined such that $u=\partial\psi/\partial y$ and $v=-\partial\psi/\partial x$. The vorticity is defined by $\omega=\partial u/\partial y-\partial v/\partial x$. Based on this definition, the initial and boundary conditions for the stream function and the vorticity can be written as

$$\begin{aligned}
&\psi=0, \quad \omega=0 && \text{at } \tau=0\\
&\psi=0, \quad \omega=\partial^2\psi/\partial x^2 && \text{at } x=0 \text{ and } 1\\
&\psi=0, \quad \omega=\partial^2\psi/\partial y^2 && \text{at } y=0\\
&\psi=0, \quad \omega=0 && \text{at } y=s.
\end{aligned} \quad (10)$$

Note that in equation (8) the simple notations $\mu_x=\partial\mu/\partial x$ and $\mu_y=\partial\mu/\partial y$ have been used. The parameter $Gr^*=\rho^2 g\beta(\Lambda_0-\Lambda_s)L^3/(C_p)_l(\mu_l^*)^2$ is a modified Grashof number and $c_p=C_p/(C_p)_l$ is a dimensionless specific heat. It appears that equation (8) reduces to $\nabla^2\omega=0$ in the solid phase, if the viscosity of the solid phase is assumed uniform and infinite. Thus, the vorticity will be zero in the solid phase as long as the vorticity has a zero value at all of the boundaries of the solid phase. In equation (9), the artificial viscosity γ and the dimensionless latent heat f are defined by

$$\gamma=\infty \quad \text{and} \quad f=0 \quad \text{if} \quad \lambda\leqslant\lambda_f \quad (11a)$$

$$\gamma=1 \quad \text{and} \quad f=1 \quad \text{if} \quad \lambda>\lambda_f \quad (11b)$$

for the solid and liquid phase, respectively. Hence, equation (9) guarantees a zero velocity field for the solid phase due to an infinite viscosity, whereas for the liquid phase, equation (9) becomes the stream function equation as in conventional stream–vorticity formulations. The use of the artificial viscosity γ is very important in treating the discontinuity of the velocity gradient normal to the liquid–solid interface. This will be demonstrated later. Mathematically, equation (9) can be applied on the entire physical domain including the liquid–solid interface. When a numerical scheme is applied, however, the f-value possesses a discontinuity inside a finite control volume covering both liquid and solid phases. Thus, care must be exercised in evaluating the f-value for such a control volume.

Equation (9), in fact, is identical to heat conduction in a two-dimensional composite material with heat generation if the liquid and the solid phases are treated as two different materials and the stream function ψ and the vorticity ω are regarded as temperature and heat sink, respectively. It is noted that the vorticity ω has a finite value in the liquid phase and a zero value in the solid phase (due to a zero velocity). Thus, the heat sink is needed to consider for the liquid phase only. For convenience, the value of the vorticity in the solid phase of a finite control volume covering both liquid and solid phases is assumed equal to that of the liquid phase inside this same control volume. Such an assumption would overestimate the heat sink for that control volume. Therefore, this heat sink should be multiplied by the liquid fraction inside the control volume. This can be achieved easily by treating the f-value appearing in equation (9) as the liquid fraction inside the control volume. A simple method for the evaluation of the f-value can be found in ref. [22].

METHOD OF SOLUTION

Equations (5), (8) and (9) along with the boundary conditions (6) and (10) constitute a system of coupled non-linear partial differential equations. In this system of equations, both real and artificial viscosities (μ and γ) have an infinite value in the solid phase. Thus, there exists sharp discontinuities in the μ and γ values at the liquid–solid interface. Fortunately, such discontinuities can be effectively handled by the use of the weighting function scheme developed in ref. [22].

Figure 1 shows a grid with schematic liquid–solid interfaces. The dashed curve represents an interface such that point P is located in the solid region, whereas the solid curve stands for the case that point P is in the liquid region. Based on the symbols defined in Fig. 1, the weighting function scheme [22] for equation (9) can be expressed as

$$a_W\psi_W+a_E\psi_E+a_S\psi_S+a_N\psi_N+a_P\psi_P=a_R$$
$$a_W=(W_i\Delta x_i)^{-1}, \quad a_E=(E_i\Delta x_i)^{-1}$$
$$a_S=(S_j\Delta y_j)^{-1}, \quad a_N=(N_j\Delta y_j)^{-1}$$
$$a_P=-a_W-a_E-a_S-a_N, \quad a_R=(f\omega)_{i,j}$$
$$W_i=\int_W^P\frac{1}{\gamma}\,dx, \quad E_i=\int_P^E\frac{1}{\gamma}\,dx$$
$$S_j=\int_S^P\frac{1}{\gamma}\,dy, \quad N_j=\int_P^N\frac{1}{\gamma}\,dy. \quad (12)$$

The notation used here is the same as that in ref. [22]. For convenience, however, the names of the grid points are used to define the boundaries of the integrals. Suppose the interface passes through points N* and W* (see the dashed curve) such that points P, S and E are located in the solid region while points W and N are in the liquid region. From equations (12), one sees that the 'thermal resistances' are

$$W_i=\overline{WW^*}+\overline{W^*P}/\gamma=\overline{WW^*}, \quad E_i=\overline{PE}/\gamma=0$$
$$S_j=\overline{SP}/\gamma=0, \quad N_j=\overline{PN^*}/\gamma+\overline{N^*N}=\overline{N^*N} \quad (13)$$

where $\overline{AB}$ denotes the distance between points A and B. Obviously, the thermal resistance is zero in the

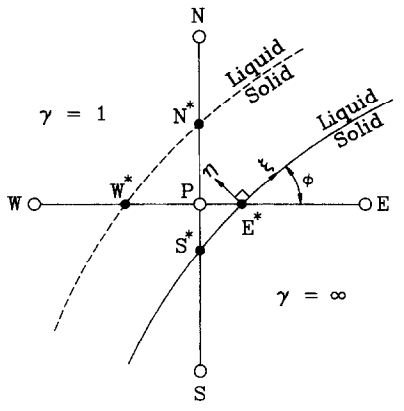

FIG. 1. A grid cell with a schematic liquid–solid interface in case point P is in solid phase (dashed curve) and point P is in liquid phase (solid curve).

intervals P–S and P–E due to a perfect 'thermal conductivity' ($\gamma = \infty$), whereas that in the intervals P–N and P–W is non-zero. Under such a situation, the weighting factors a_W and a_N will be negligibly small as compared to $a_S = \infty$ and $a_E = \infty$. As a result, the ψ-value in the solid region (point P) is independent of that in the liquid region. This leads to $\psi = 0$ for the solid phase due to the homogeneous boundary conditions (10) around the solid region. Thus, the ψ-value at a point can be directly assigned zero if that point is located in the solid region. In case point P is in the liquid phase when the interface goes through points E* and S* as illustrated by the solid curve, the total 'thermal resistances' become

$$W_i = \overline{WP}, \quad E_i = \overline{PE^*} + \overline{E^*E}/\gamma = \overline{PE^*}$$
$$S_j = \overline{SS^*}/\gamma + \overline{S^*P} = \overline{S^*P}, \quad N_j = \overline{PN}. \qquad (14)$$

From equations (14), one sees that the thermal resistance in the interval P–E is equal to that in the interval P–E* due to a perfect thermal conductivity in the interval E*–E. This is equivalent to assigning $\psi_{E^*} = \psi_E = 0$. Generally speaking, the ψ-value at point P would not be zero such that a discontinuity in the velocity gradient exists at the interface. This will cause a vorticity discontinuity across the liquid–solid interface. When points W, E, S, N and P are all at the liquid phase, equation (9) reduces to $\nabla^2\psi = \omega$ such that it can be solved as in a conventional problem without phase change.

Like the stream function, the vorticity in the solid phase is identically zero. On the liquid side of the liquid–solid interface, however, there exists a non-zero boundary vorticity due to a friction force arising from the no-slip condition. This implies that the vorticity is not a continuous function across the liquid–solid interface. Thus, the boundary vorticity at the interface must be estimated before equation (8) is solved. To accomplish this, let (ξ, η) be local orthogonal coordinates located at point E* with η normal to the interface represented by the solid curve as shown in Fig. 1. Assume the grid cell is sufficiently small such that the profile of the liquid–solid interface inside the grid cell can be approximated with a straight line. Based on this, the boundary vorticity at point E* is computed from

$$\omega_{E^*} = \partial^2\psi/\partial x^2 + \partial^2\psi/\partial y^2 = \partial^2\psi/\partial\eta^2 \qquad (15a)$$

or

$$\omega_{E^*} = (\sin^{-2}\phi)\,\partial^2\psi/\partial x^2 \qquad (15b)$$

where ϕ is the inclination angle of the liquid–solid interface measured from the horizontal. Similarly, the boundary vorticity at point S* is

$$\omega_{S^*} = (\cos^{-2}\phi)\,\partial^2\psi/\partial y^2. \qquad (16)$$

In the solution procedure, the vorticity at point E is assigned as $\omega_E = \omega_{E^*}$ while the concept of infinite viscosity is applied in the interval E*–E. It should be noted also that all of the vorticity in the solid region must be directly assigned zero except for a few points near the interface like point E. This treatment is only for numerical convenience. The real vorticity, however, is still zero at point E. After equations (5) and (8) are discretized by the use of the weighting function scheme [22], the resulting algebraic equations as well as equations (12)–(14) for the stream function can be solved by the SIS solver [25]. At each time step, the computations should be repeated until the solutions satisfy the convergence criteria

$$\frac{\text{Max}\,|\psi - \psi^0|}{|\text{Max}\,\psi - \text{Min}\,\psi|} \leqslant \varepsilon_\psi \qquad (17a)$$

$$\frac{\text{Max}\,|\omega - \omega^0|}{|\text{Max}\,\omega - \text{Min}\,\omega|} \leqslant \varepsilon_\omega \qquad (17b)$$

$$\text{Max}\,|\lambda - \lambda^0| \leqslant \varepsilon_\lambda \qquad (17c)$$

where ψ^0, ω^0 and λ^0 denote the solutions at the previous iteration. The values of the tolerances ε_ψ, ε_ω and ε_λ are not necessarily the same. For convenience, the present algorithm is summarized as follows.

(1) Guess $\lambda(x, y)$ and $\omega(x, y)$ at time τ.

(2) Locate the interface and compute the f-value for each control volume.

(3) Solve the stream function $\psi(x, y)$ from equations (12)–(14).

(4) Evaluate the velocity components by $u = \partial\psi/\partial y$ and $v = -\partial\psi/\partial x$.

(5) Find the vorticity along the boundaries of the liquid region and solve equation (8) to obtain $\omega(x, y)$.

(6) Renew $\lambda(x, y)$ from equation (5).

(7) Check the convergence criteria (17). If the criteria are satisfied, then go to the next step. Otherwise, return to step 2.

(8) If $\tau = \tau_{max}$, then stop the computations. Otherwise, let $\psi_0 = \psi$, $\omega_0 = \omega$, $\lambda_0 = \lambda$ and $f_0 = f$ and return to step 1 for the next time step.

RESULTS AND DISCUSSION

Numerical results were obtained for the cases of $(T_0, T_\infty) = (233°C, 229°C)$, $(233°C, 226°C)$ and

Table 1. Thermophysical properties of pure tin

Freezing point $T_f = 231.9$°C	
Density $\rho_l = 6992$ kg m^{-3}	
Latent heat $\Delta H = 59.50$ kJ kg^{-1}	
Expansion coefficient $\beta = 1.060 \times 10^{-4}$ K^{-1}	
Dynamic thermal diffusivity [kg m^{-1} s^{-1}]	
$\kappa = 0.2923 - 3.695 \times 10^{-4} T$	$T \leqslant 231.9$
$\kappa = 0.1011 + 7.59 \times 10^{-5} T$	$T \geqslant 231.9$
Specific heat [J kg^{-1} K^{-1}]	
$C_P = 215.1 + 0.22T$	$T \leqslant 231.9$
$C_P = 255.4$	$T \geqslant 231.9$
Dynamic viscosity [kg m^{-1} s^{-1}]	
$\mu^* = \infty$	$T \leqslant 231.9$
$\mu^* = 3.004 \times 10^{-3} - 5.53 \times 10^{-6} T + 3.74 \times 10^{-9} T^2$	$T \geqslant 231.9$
Prandtl number	
$Pr = \infty$	$T \leqslant 231.9$
$Pr = 2.729 \times 10^{-2} - 5.713 \times 10^{-5} T + 3.89 \times 10^{-8} T^2$	$T \geqslant 231.9$

(234°C, 226°C) in an enclosure having the size $L = 8.89$ cm and the aspect ratio $s = 0.75$. Their corresponding (Ste, Gr^*, λ_f) values are, respectively, (0.0177, 3.977×10^7, 0.7329), (0.0310, 6.985×10^7, 0.8479) and (0.0353, 7.950×10^7, 0.7449). These ranges of temperature give rise to a superheat in the liquid phase and a subcool in the solid phase (i.e. $T_f = 231.9$°C for pure tin). Table 1 shows the thermophysical properties of the pure tin used in the computations. The Prandtl number Pr_l in the energy equation (5) has the value of 0.01613 for pure tin. Such information has been well documented in the literature [26, 27].

Figure 2 reveals the streamlines for the case of (T_0, T_s) = (233°C, 229°C) at $t = 0.165$ and 1.896 h. The minimum ψ-value in Fig. 2(a) is -409.5. This means that the natural convection at $t = 0.165$ h is a clockwise circulating flow with a strength of 409.5. The liquid tin near the interface (where $\psi = 0$) is cooled such that it gains a downward velocity due to an increase in the density. In contrast, the liquid tin obtained an upward driving force on the vicinity of the heated wall ($x = 0$). Thus, a clockwise circulating flow forms in the liquid region. At $t = 1.896$ h, the strength of the natural convection reduces to 249.4 owing to the diminishing of the liquid phase as observable from Fig. 2(b).

The corresponding isotherms (λ = constant) of Fig. 2 are presented in Fig. 3. The dashed curve labelled with $\lambda = 0.7329$ is the liquid–solid interface. As shown in Fig. 3(a), the interface profile is essentially a vertical straight line at $t = 0.165$ h. However, the strong circulating flow distorts the isotherms in the liquid region. In a region near the top surface, the hot liquid flows from the heated wall towards the interface. The isotherms having $\lambda = 0.9$ thus bends to the right. This causes a large temperature gradient normal to the interface such that the solidification rate is depressed. With a similar reasoning, the solidification has a faster speed at the bottom of the enclosure. Therefore, the liquid–solid interface has a sinuous profile at $t = 1.896$ h (see Figs. 2(b) and 3(b)).

As mentioned earlier, a no-slip velocity prevails at the top of the liquid at the very beginning of the solidification process. This particular boundary condition will retard the fluid flow. Thus, a faster sol-

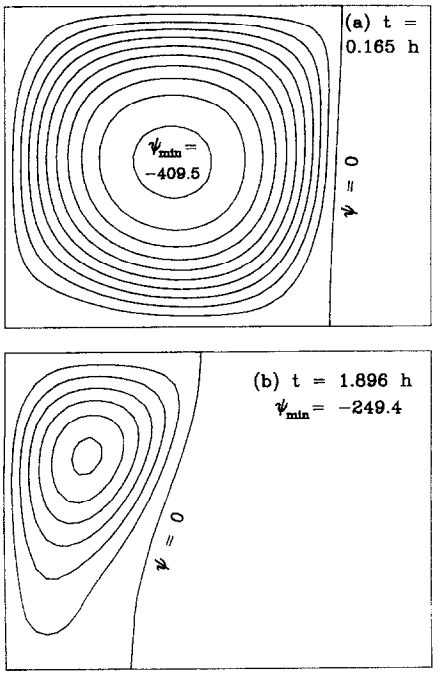

FIG. 2. Streamlines with an increment of $\Delta\psi = 40$ for (T_0, T_s) = (233°C, 229°C) at (a) $t = 0.165$ h and (b) $t = 1.896$ h.

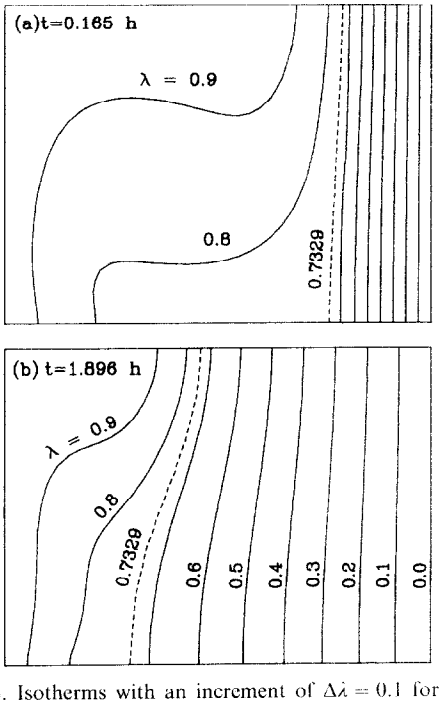

FIG. 3. Isotherms with an increment of $\Delta\lambda = 0.1$ for (T_0, T_s) = (233°C, 229°C) at (a) $t = 0.165$ h and (b) $t = 1.896$ h.

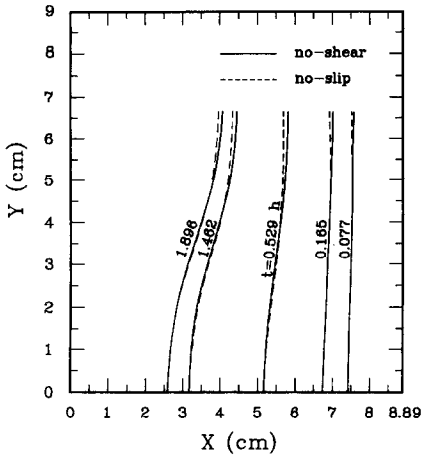

FIG. 4. Interface profiles for (T_0, T_∞) = (233°C, 229°C) at t = 0.077, 0.165, 0.529, 1.462 and 1.896 h (from right to left).

idification speed at the top of the liquid can be expected if the no-slip boundary condition is used instead of the no-shear boundary condition. To examine such a difference, the interface profiles based on each of the two different boundary conditions are compared in Fig. 4. The five curves from right to left are, respectively, for t = 0.077, 0.165, 0.529, 1.462 and 1.896 h. From Fig. 4, one sees that the interface profiles indeed are not very sensitive to this boundary condition.

Figure 5 shows comparisons of the present interface profiles (no-shear) with the numerical results and the experimental data of Wolff and Viskanta [7]. The experimental data [7] are denoted with symbols. Again, the five interface profiles of each result are for t = 0.077, 0.165, 0.529, 1.462 and 1.896 h (from right to left). However, the numerical predictions of Wolff and Viskanta [7] (the dashed curve) was only up to t = 1.462 h. In their numerical study, Wolff and Viskanta [7] employed the two-region method [5] with

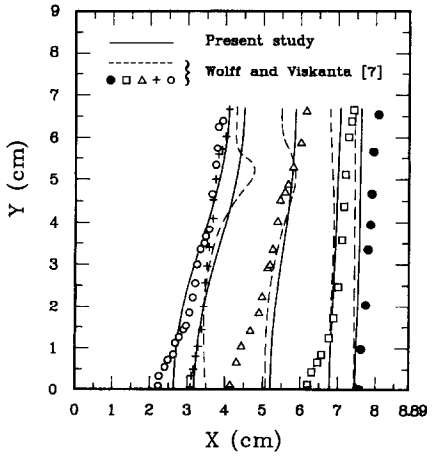

FIG. 5. Comparisons of interface profiles for (T_0, T_∞) = (233°C, 229°C) at t = 0.077, 0.165, 0.529, 1.462 and 1.896 h (from right to left).

the assumption that the curvature of the interface profile was negligibly small. Unfortunately, this assumption led to an interface having a cavity of larger curvature at t = 1.462 h (see Fig. 5). In fact, no cavity could be found in the experiment. Wolff and Viskanta [7] attributed this cavity to the no-slip boundary condition employed in their computation. However, in the use of the present numerical technique both no-slip and no-shear boundary conditions do not give rise to any cavity on the interface (see Fig. 4). Thus, the cavity predicted in ref. [7] is believed to arise from the numerical error of the two-region method employed [5].

From Fig. 5, one sees also that the measured data has a smaller value than the present prediction does at the earlier times t = 0.077 and 0.165 h. This might be attributed to the thermal inertia of the experimental setup. As reported by Wolff and Viskanta [7], in their experiment approximately 0.033 h (0.033/0.077 = 42.9%) elapsed before the desired temperature T_∞ was reached at the cold wall. Also, at the bottom of the test region the imperfect insulation might have speeded up the solidification rate as remarked by Wolff and Viskanta [7]. This might account for the fact that the measured solidification thickness is larger than that of the present prediction in the vicinity of the Pyrex glass plate that forms the bottom of the test region (y = 0), especially at t = 0.529 h. At a later time, say t = 1.896 h, the liquid region becomes quite narrow while its superheat is still maintained at $T_0 - T_f$ = 1.1°C. This implies that the horizontal temperature gradient in the liquid region would increase as the solidification proceeds. The solidification speed thus is depressed until an equilibrium solidification thickness is accomplished eventually. Under this situation, the heat loss from the bottom could be compensated by the heating boundary condition imposed at x = 0. Thus, good agreement between the experimental data [7] and the present prediction can be once again observed at t = 1.896 h.

To examine the uncertainty in Wolff and Viskanta's experimental data [7], their measured solid-phase thickness vs time is presented in Fig. 6 for the three representative heights y/s = 0.0, 0.5 and 1.0. The present result is also plotted in Fig. 6 for comparisons. From Fig. 6, it is seen that the present numerical method predicts a smoothly increasing solid thickness with a decreasing solidification speed. This is consistent with the physical reasoning for a PCM having a distinct freezing point (see Fig. 4 of ref. [22]). The measured solid thickness, however, has a zigzag variation in the time coordinate especially at the bottom of the test region (y = 0). Nevertheless, a qualitative agreement between the present predictions and the experimental data [7] is observable from Fig. 5.

The predicted liquid temperatures based on no-shear and no-slip conditions are compared with the measured data in Fig. 7 for t = 0.077 h and in Fig. 8 for t = 0.529 h. Figures 7 and 8 clearly reveal that the no-shear condition decreases the temperature due to

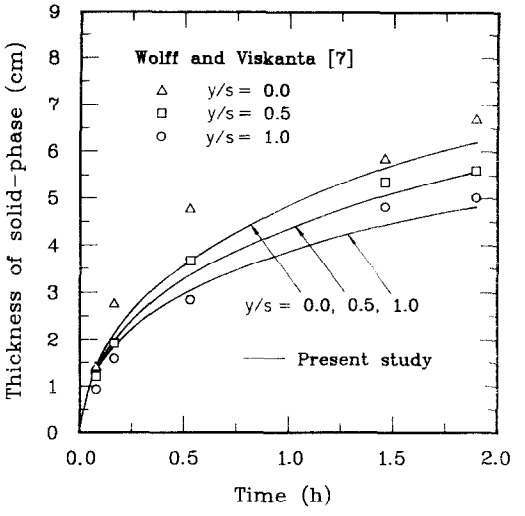

Fig. 6. Variation of solid thickness at $y/s = 0.0$, 0.5 and 1.0 for the case $(T_0, T_c) = (233\,^{\circ}\mathrm{C}, 229\,^{\circ}\mathrm{C})$.

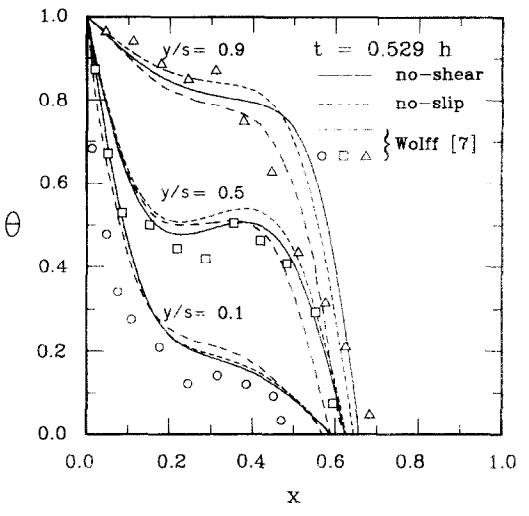

Fig. 8. Comparison of liquid temperatures for $y/s = 0.1$, 0.5 and 0.9 at $t = 0.529$ h.

an enhanced heat transfer. However, it gives rise to a larger temperature gradient normal to the interface at the height $y/s = 0.9$. This is the major reasoning why the solidification speed based on no-shear is slower than that based on no-slip, although it is not so significant (see Fig. 4). From Fig. 7, the measured data are seen to be considerably smaller than the predictions. Fortunately, this discrepancy is greatly improved in the region of $y/s > 0.5$ at a later time $t = 0.529$ h as shown in Fig. 8. In fact, the discrepancy between the measured temperature and the prediction is within the error of the measurement. The thermocouple used by Wolff and Viskanta [7] has an accuracy of $\pm 0.1\,^{\circ}\mathrm{C}$ whereas the superheat in the liquid tin of their experiment is only $1.1\,^{\circ}\mathrm{C}$.

To investigate the effect of the subcool in solid, the computations were repeated with $T_c = 226\,^{\circ}\mathrm{C}$. This implies that the subcool in the solid is increased from 2.9 to $5.9\,^{\circ}\mathrm{C}$ while the superheat is maintained at $1.1\,^{\circ}\mathrm{C}$. Figure 9 illustrates the resulting interface profiles based on the no-shear condition for various time instants $t = 0.077$, 0.165, 0.529, 0.799 and 0.931 h (from right to left). The measured data [7] for the same time instants are also plotted in Fig. 9 for comparison. A similar work for the case $(T_0, T_c) = (234\,^{\circ}\mathrm{C}, 226\,^{\circ}\mathrm{C})$ was performed to study the effect of superheat in the liquid. The results of interface profiles are shown in Fig. 10 for $t = 0.077$, 0.165, 0.529, 1.146 and 1.462 h (from right to left). In the latter case, the superheat in the liquid and the subcool in the solid are, respectively, 2.1 and $5.9\,^{\circ}\mathrm{C}$.

On comparing the predictions in Fig. 9 with that in Fig. 5, one sees that increasing the subcool of the solid will speed up the solidification. This gives rise to a faster diminishing for the liquid region such that the effect of the natural convection in the liquid region is decreased. Thus, the interface profiles in Fig. 9 are

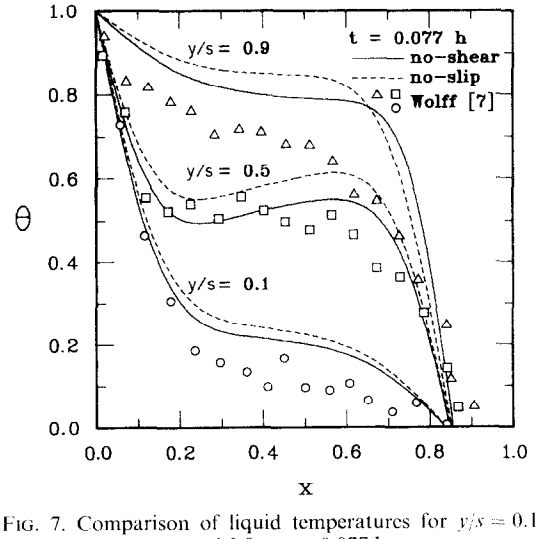

Fig. 7. Comparison of liquid temperatures for $y/s = 0.1$, 0.5 and 0.9 at $t = 0.077$ h.

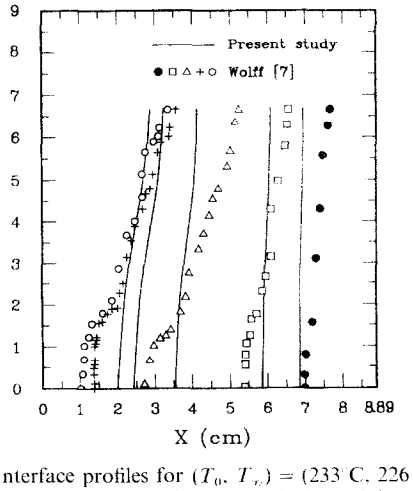

Fig. 9. Interface profiles for $(T_0, T_c) = (233\,^{\circ}\mathrm{C}, 226\,^{\circ}\mathrm{C})$ at $t = 0.077$, 0.165, 0.529, 0.799 and 0.931 h (from right to left).

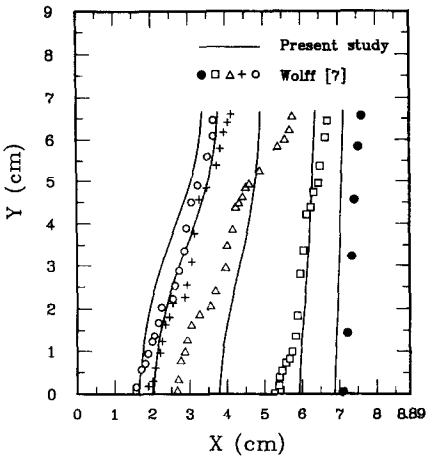

FIG. 10. Interface profiles for $(T_0, T_\infty) = (234°C, 226°C)$ at $t = 0.077, 0.165, 0.529, 1.146$ and 1.462 h (from right to left).

flatter than that in Fig. 5. This trend is reversed when the superheat in the liquid is increased as can be seen by comparing the predictions in Figs. 9 and 10. As pointed out by Wolff and Viskanta [7], the heat loss from the bottom of the test region could be an important error source for their measurement. This is even worse when the subcool of the solid is increased (see the measured data at $y = 0$ and $t = 0.931$ h in Fig. 9). It is interesting to note that the results presented in Fig. 10 are based on both large superheat and large subcool. As a result, the heat loss enhances the solidification speed in the vicinity of $y = 0$ at earlier time ($t < 0.529$ h). At later time ($t > 1.146$ h), however, the heated wall ($x = 0$) has a strong depression on the solidification as mentioned earlier. This might account for the fact that the agreement between the measured data and the present prediction in Fig. 10 is quite good at the initial and final times, but very poor at intermediate times.

In the present computations, a uniform grid system with 41×31 grid points (i.e. $\Delta x = \Delta y = 0.025$) was used for the first case $(T_0, T_\infty) = (233°C, 229°C)$. However, the numerical solutions were found essentially unchanged when the step size was doubled (21×16 points). Hence, the step size $\Delta x = \Delta y = 0.050$ was employed for the other two cases $(T_0, T_\infty) = (233°C, 226°C)$ and $(234°C, 226°C)$. A variable step size was employed in the time coordinate such that numerical results for some particular time instants (e.g. $t = 0.077, 0.165, 0.529, 1.462$ and 1.896 h) could be obtained. Fortunately, the numerical solution was not sensitive to the time steps either. Hence, large time step sizes (only 32 time steps for Fig. 4, 35 steps for Fig. 9 and 50 steps for Fig. 10) were used in the present computations. For the present problem, the optimum SOR values required by the SIS solver [25] were found in the range of 0.2–0.6 for the stream function, 0.1–0.3 for the vorticity and 0.1–0.25 for the enthalpy. In all of the computations, the convergence criterion $\varepsilon_\psi = \varepsilon_\omega = 0.005$ and $\varepsilon_\lambda = 0.0005$ was used.

In their numerical study, Wolff and Viskanta [7] employed the two-region method [5] with stream–vorticity formulation for the liquid flow. A grid system having 31×31 grid points was used in each of the liquid and solid regions for the case of $(T_0, T_\infty) = (233°C, 229°C)$. Numerical results were obtained only up to $t = 1.462$ h. For such a computation, a very large computational cost (7.08 CPU h on a CYBER 205 supercomputer) was reported. Hence, only one case was computed in their study. In the use of the present method, however, only 0.73 CPU h were required on a CYBER 840 computer for this same case with 41×31 grid points and 32 time steps (up to $t = 1.896$ h). Thus, the computation effort needed by the present method is less than 2% of that needed in ref. [7]. The high efficiency of the present method seems to come from the combined effects of the particular treatment on the latent heat [22], the single-region formulation with the weighting function scheme [22] and a strongly implicit solver [25]. As a final note, it is mentioned that the present numerical technique produces smooth streamlines and isotherms (λ = constant) even in the vicinity of the liquid–solid interface. This is a unique feature of the present numerical technique among the existing single-region methods [9–15].

CONCLUSIONS

The enthalpy formulation developed in ref. [22] is extended in the present investigation for convection–conduction phase change problems. The solid phase is regarded as a liquid of infinite viscosity. The weighting function scheme then is employed to treat the sharp viscosity jump across the liquid–solid interface. Also, an artificial viscosity is introduced to the stream function equation to allow for a shear stress at the interface. From the results of computations for a solidification of pure tin, the following conclusions can be drawn:

(1) Unlike the existing single-region methods, the present numerical technique produces smooth streamlines and isotherms even in the vicinity of the liquid–solid interface.

(2) The present predictions are not sensitive to the spatial and time step sizes.

(3) The computation effort required by the present technique is less than 2% of that needed by the two-region method [7] for the same problem.

(4) No cavity is predicted at the liquid–solid interface. This agrees with the experimental data [7]. Thus, the cavity produced by the two-region method [7] at the liquid–solid interface is believed to arise from numerical errors.

Acknowledgement—The authors wish to express their appreciation to the National Science Council of the Republic of China in Taiwan for the financial support of this work through the project NSC78-0401-E007-09.

REFERENCES

1. W. C. Winegard and G. S. Cole, Thermal convection during horizontal solidification of pure metals and alloys, *J. Inst. Metals* **93,** 153–164 (1964).
2. J. Szekely and P. S. Chhabra, The effect of natural convection on the shape and movement of the melt solid interface in the controlled solidification of lead, *Metall. Trans.* **1,** 1195–1203 (1970).
3. F. M. Chiesa and R. I. L. Guthrie, Natural convection heat transfer rate during solidification and melting of metals and alloys systems, *ASME J. Heat Transfer* **96,** 377–384 (1974).
4. E. M. Sparrow, S. V. Patankar and S. Ramadhyani, Analysis of melting in the presence of natural convection in the melt region, *ASME J. Heat Transfer* **99,** 520–526 (1977).
5. N. Ramachandran, J. P. Gupta and Y. Jaluria, Thermal and fluid flow effects during solidification in a rectangular enclosure, *Int. J. Heat Mass Transfer* **25,** 187–194 (1982).
6. B. W. Webb and R. Viskanta, Analysis of heat transfer during melting of a pure metal from an isothermal vertical wall, *Numer. Heat Transfer* **9,** 539–558 (1986).
7. F. Wolff and R. Viskanta, Solidification of a pure metal at a vertical wall in the presence of liquid superheat, *Int. J. Heat Mass Transfer* **31,** 1735–1744 (1988).
8. P. G. Kroeger and S. Ostrach, The solution of a two-dimensional freezing problem including convection effects in the liquid region, *Int. J. Heat Mass Transfer* **17,** 1191–1207 (1974).
9. G. E. Schneider, Computation of heat transfer with solid/liquid phase change including free convection, *AIAA J. Thermophys. Heat Transfer* **1,** 136–145 (1987).
10. V. R. Voller, M. Cross and N. C. Markatos, An enthalpy method for convection/diffusion phase change, *Int. J. Numer. Meth. Engng* **24,** 271–284 (1987).
11. V. R. Voller and C. Prakash, A fixed grid numerical modelling methodology for convection–diffusion mushy region phase-change problems, *Int. J. Heat Mass Transfer* **30,** 1709–1719 (1987).
12. W. D. Bennon and F. P. Incropera, A continuous model for momentum, heat and species transfer in binary solid–liquid phase change systems—I. Model formulation, *Int. J. Heat Mass Transfer* **30,** 2161–2170 (1987).
13. W. D. Bennon and F. P. Incropera, A continuum model for momentum, heat and species transfer in binary solid–liquid phase change systems—II. Application to solidification in a rectangular cavity, *Int. J. Heat Mass Transfer* **30,** 2171–2187 (1987).
14. C. Beckermann and R. Viskanta, Natural convection solid/liquid phase change in porous media, *Int. J. Heat Mass Transfer* **31,** 35–46 (1988).
15. A. D. Brent, V. R. Voller and K. J. Reid, Enthalpy–porosity technique for modeling convection–diffusion phase change: application to the melting of a pure metal, *Numer. Heat Transfer* **13,** 297–318 (1988).
16. M. A. Hastaoglu, Numerical solution of three-dimensional moving boundary problem: melting and solidification with blanketing of a third layer, *Chem. Engng Sci.* **42,** 2417–2423 (1987).
17. N. Shamsundar and E. M. Sparrow, Analysis of multidimensional conduction phase change via the enthalpy model, *ASME J. Heat Transfer* **97,** 333–340 (1975).
18. G. E. Schneider and M. Zedan, A coupled modified strongly implicit procedure for the numerical solution of coupled continuum problem, AIAA Paper 84-1743 (1984).
19. M. J. Raw and G. E. Schneider, A new implicit solution procedure for multidimensional finite-difference modeling of the Stefan problem, *Numer. Heat Transfer* **8,** 559–571 (1985).
20. S. V. Patankar, *Numerical Heat Transfer and Fluid Flow*. Hemisphere, Washington, DC (1980).
21. R. Viskanta, Heat transfer during melting and solidification of metals, *ASME J. Heat Transfer* **110,** 1205–1219 (1988).
22. S. L. Lee and R. Y. Tzong, An enthalpy formulation for phase change problems with a large thermal diffusivity jump across the interface, *Int. J. Heat Mass Transfer* **34,** 1491–1502 (1991).
23. M. C. Flemings, *Solidification Processing*, p. 167. McGraw-Hill, New York (1974).
24. R. H. F. Pao, *Fluid Dynamics*, p. 280. Charles E. Merrill Books, Columbus, Ohio (1967).
25. S. L. Lee, A strongly implicit solver for two-dimensional elliptic differential equations, *Numer. Heat Transfer* **16B,** 161–178 (1989).
26. S. S. Kutateladze, V. M. Borishanskii, I. I. Novikov and O. S. Fedynskii, *Liquid Metal Heat Transfer Media*. Consultants Bureau, New York (1959).
27. W. H. Cubberly, *Metals Handbook*, 9th Edn, Vol. 2, pp. 811–814. ASM, Metal Park, Ohio (1979).

APPLICATION DU SCHEMA DES FONCTIONS DE PONDERATION AUX PROBLEMES DE CONDUCTION–CONVECTION AVEC CHANGEMENT DE PHASE

Résumé—Une formulation numérique basée sur le schéma des fonctions de pondération est développée pour les problèmes de conduction–convection avec changement de phase. La phase solide est considérée comme un liquide ayant une viscosité infinie. Cela permet d'appliquer la formulation fonction de courant–vorticité à tout le domaine physique en incluant l'interface liquide–solide. Un problème avec de l'étain pur est considéré pour tester les performances de la présente méthode. Les profils calculés de l'interface s'accordent qualitativement avec les données expérimentales disponibles. L'investissement de calcul est de 2% inférieur à ce que demande la méthode des deux régions pour le même problème. Contrairement aux méthodes existantes à une seule région, les lignes de courant et les isothermes sont continues même au voisinage du front de solidification.

ANWENDUNG VON GEWICHTUNGSFUNKTIONEN AUF PROBLEME DES PHASENWECHSELS MIT KONVEKTION UND WÄRMELEITUNG

Zusammenfassung—Die vorliegende Untersuchung beschäftigt sich mit Konvektion und Wärmeleitung beim Phasenwechsel. Hierzu wird mit Hilfe von Gewichtungsfunktionen ein numerischer Ansatz formuliert. Die feste Phase wird als Flüssigkeit mit unendlich großer Zähigkeit betrachtet. Dieses Vorgehen erlaubt die Anwendung des Stromfunktion-Wirbeltransport-Verfahrens im gesamten Bereich einschließlich der flüssig/festen Grenzfläche. Die Gewichtungsfunktionen werden zur Darstellung des starken Zähigkeitssprunges an der flüssig/festen Grenzfläche angewandt. An einem Beispiel mit reinem Zinn wird die vorliegende Methode überprüft. Die ermittelten Grenzflächenprofile stimmen qualitativ mit verfügbaren Versuchswerten überein. Der Rechenaufwand für das hier entwickelte numerische Verfahren ist geringer als 2% dessen bei der Zweizonenmethode für dasselbe Problem. Im Gegensatz zu den bestehenden Einzonenmethoden liefert das vorliegende numerische Verfahren glatte Stromlinien und Isothermen—selbst in der Umgebung der Verfestigungsfront.

ПРИМЕНЕНИЕ СХЕМЫ С ВЕСОВЫМИ ФУНКЦИЯМИ К ЗАДАЧАМ ФАЗОВОГО ПРЕВРАЩЕНИЯ ПРИ НАЛИЧИИ КОНВЕКЦИИ И ТЕПЛОПРОВОДНОСТИ

Аннотация—Предложен подход к численному решению задач фазового превращения при наличии конвекции и теплопроводности, основанный на схеме с весовыми функциями. Твердая фаза рассматривается как жидкость с бесконечной вязкостью. Такой подход позволяет использовать понятие завихренности потока во всей физической области, включая границу раздела жидкость–твердое тело. Эффективность предложенного метода проверяется на примере чистого олова. Расчетные профили межфазных границ качественно согласуются с имеющимися экспериментальными данными. При этом разработанный численный метод требует менее 2% от объема расчетов для двухзонального метода решения рассматриваемой задачи. В отличие от существующих однозональных методов представленный численный метод позволяет получить гладкие линии тока и изотермы даже в окрестности фронта затвердевания.